SUPPLEMENTARY INFORMATION: Ultra-High Dose-Rate Irradiation Spares DNA under Physiological Oxygen and Salt Conditions

Marc Benjamin Hahn[*,1], Sepideh Aminzadeh-Gohari[2], Anna Grebinyk[2], Matthias Gross[2], Andreas Hoffmann[2], Xiangkun Li[2], Anne Oppelt[2], Chris Richard[2], Felix Riemer[2], Frank Stephan[2], Elif Tarakci[2], and Daniel Villani[2]

[1]marc.hahn@uni-potsdam.de, Institut für Chemie, Universität Potsdam, Karl-Liebknecht-Str. 24-25, 14476 Potsdam, Germany
[2]Deutsches Elektronen-Synchrotron (DESY), Platanenallee 6, 15738 Zeuthen, Germany

Abstract

Cancer treatment with radiotherapy aims to kill tumor cells while sparing healthy tissue. Therefore, the experimentally observed sparing of healthy tissue by the FLASH effect during irradiations with ultra-high dose rates (UHDR) enables clinicians to extend the therapeutic window and enhance treatment efficiency. However, the underlying radiobiological and chemical mechanisms are far from being understood. DNA is one of the main molecular targets for radiation therapy. Ionizing radiation damage to DNA in water depends strongly on salt, pH, buffer and oxygen content of the solvent. Here we present a study of plasmid DNA pUC19, irradiated with 18 MeV electrons at conventional/low dose rates (LDR) and UHDR under tightly controlled ambient, as well as physiological oxygen conditions in phosphate-buffered saline (PBS) at pH 7.4. For the first time, a sparing effect of DNA strand-break induction between UHDR ($>10^6$ Gy/s) and LDR ($<$0.1 Gy/s) irradiated plasmid DNA under physiological oxygen, salt and pH conditions is observed for total doses above 10 Gy. Under physiological oxygen (physoxia, $\approx$5 %O_2, 40 mmHg), more single strand-breaks (SSB) and double strand-breaks (DSB) are observed when exposed to LDR, than to UHDR. This behaviour is absent for ambient oxygen conditions (normoxia, $\approx$21 %O_2, 150-160 mmHg). The experiments are accompanied by Geant4/TOPAS-nBio based particle-scattering and chemical Monte-Carlo simulations to obtain detailed information about the yields of radicals and reactive oxygen species (ROS). To explain the observed DNA sparing ef-

fect under FLASH conditions at physoxia, the following model was proposed: The interplay of O_2 with the $^{\bullet}OH$ induced hydrogen abstraction at the sugar-phosphate backbone, and the conversion of DNA base-damage to SSB, under consideration of the dose-rate dependent H_3O^+ yield *via* beta elimination processes is accounted for, to explain the observed behavior.

Supplementary Methods and Data

Contents

1 Plasmid conformation in dependence of dose

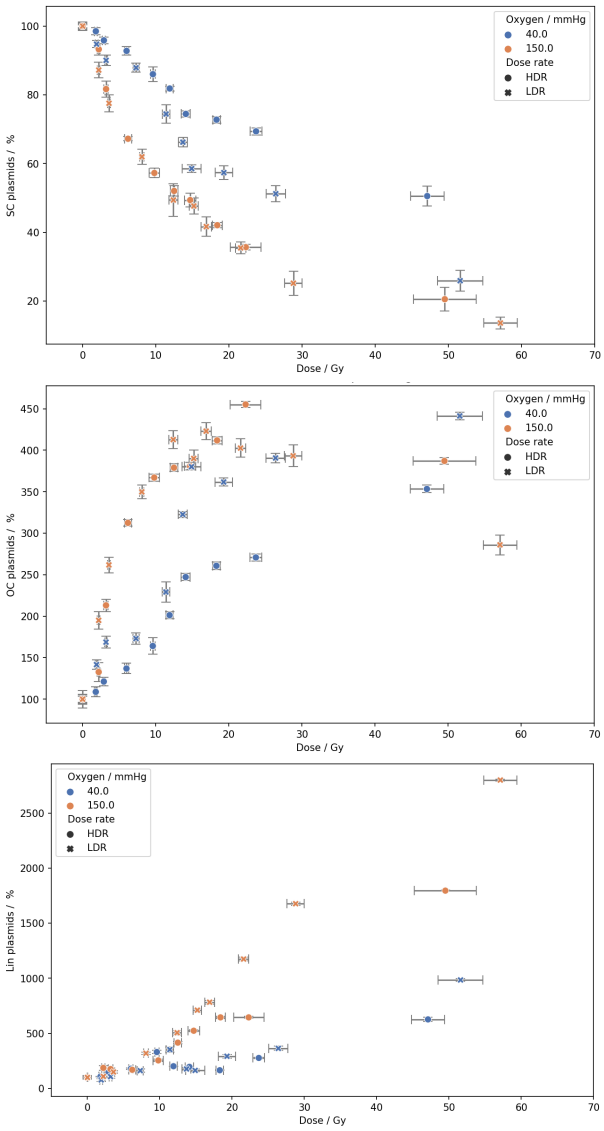

Figure S1: **Relative dose-damage response** for plasmid DNA at ambient (orange) and physiological (blue) oxygen conditions at UHDR (circles) and LDR (crosses) shown for undamaged (top), open-circular (center), and linear (bottom) DNA. The dose on the x-axis corresponds to the directly measured values from the dosimetry films and were not yet corrected by Eq.S.3

2 Simulated G-values for conventional and bunch conditions

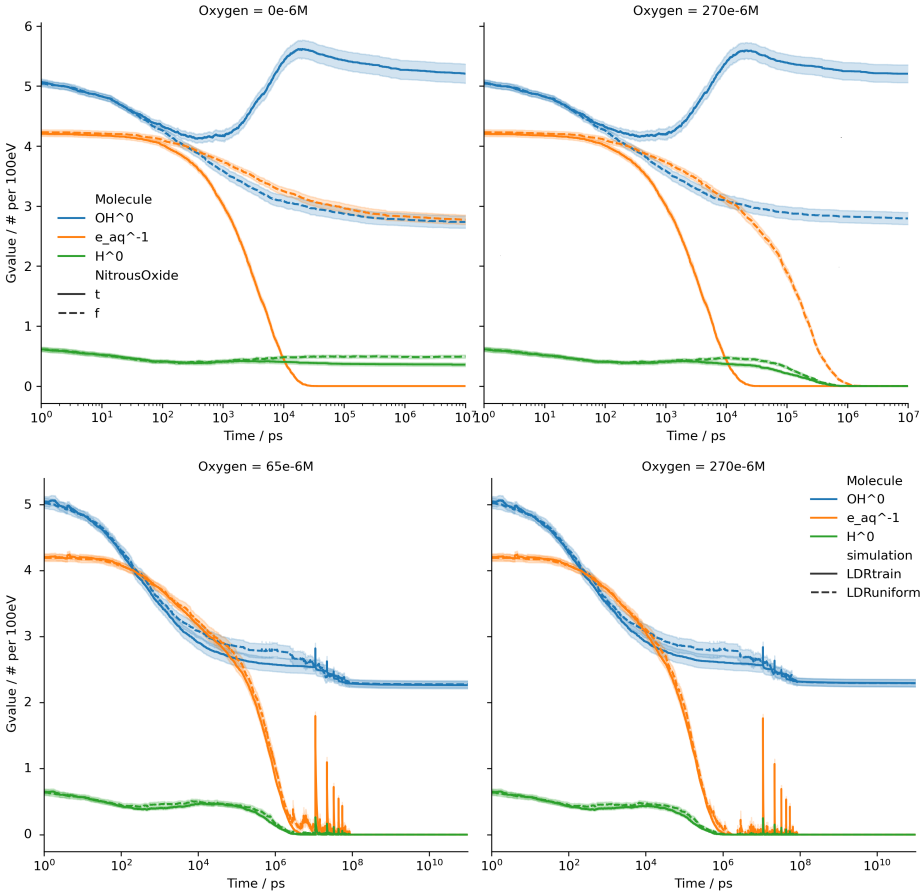

Figure S2: **G-values of the main reactive species** $^{\bullet}$OH (blue) e_{aq}^{-} (orange) and H$^{\bullet}$(green). The top shows the effect of the addition (solid line) of nitrous oxide and oxygen (right) on radical yields under standard conditions reported in the literature. On the bottom the simulation of LDR by a discrete train (solid line) and uniform structure (broken line) at physiological (left) and ambient (right) oxygen condition are compared. For details see the text.

3 Oxygen stability of sample tubes

To test the optimal sealing of the sample containers against diffusion of oxygen for future experiments under low oxygen conditions, different types of sample tubes with various sealings were prepared at oxygen levels below $<$2 mmHg (radiobiological hypoxia).[1] Therefore common Eppendorf PCR and Thermo Fisher tubes, with either snap (Eppendorf) or screw caps with o-rings (Thermo) of 0.5 mL volume were filled each with 50 μL PBS buffer. Samples were left to equilibrate in the respective oxygen conditions and atmosphere over night. These were either closed without sealing, or prepared with addition sealing of either Parafilm or Teflon, as shown exemplarily in the inset of Fig. 3. The Ep-

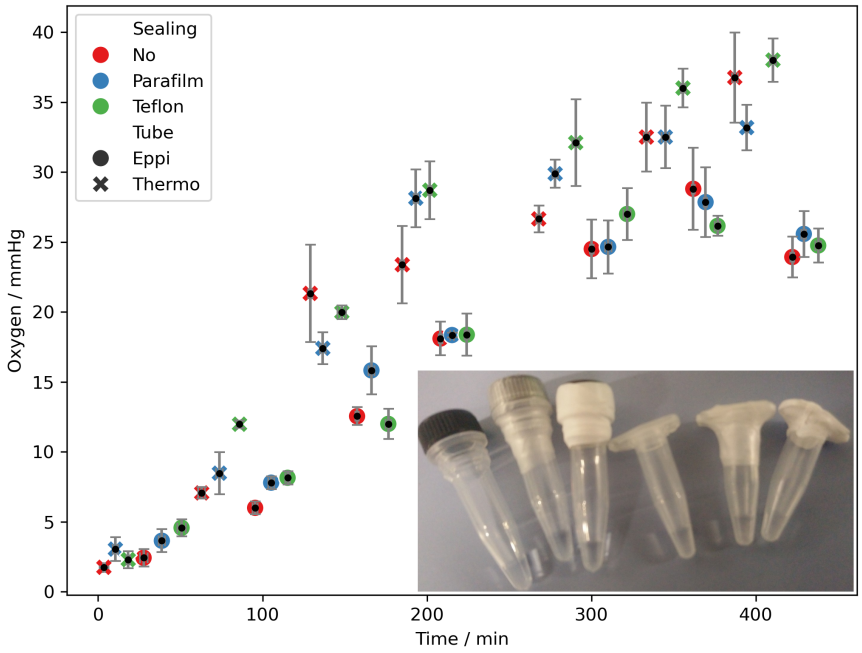

Figure S3: **Oxygen stability:** Shown is the oxygen content over time for different tubes and sealing approaches for closed sample tubes stored under ambient oxygen at room temperature, measured directly with an Oxford Oxylite oxygen sensor after opening the respective tube. The inset shows the Thermo and Eppendorf tubes without additional sealing and with Parafilm and Teflon sealing, from left to right respectively.

pendorf tubes with snap-lock provided a more efficient sealing than the Thermo tubes with screw cap for durations of about three hours at oxygen conditions around 20 mmHg oxygen in the solvent, while being exposed to ambient oxygen. The additional sealing by Teflon or Parafilm didn't show a substantial difference. Thus, to perform experiments at hypoxic conditions further improve-

ment of the sealing and/or shortest possible exposure times are needed with a stringent combined monitoring of the oxygen levels during and after the experiments.

4 Beam parameter

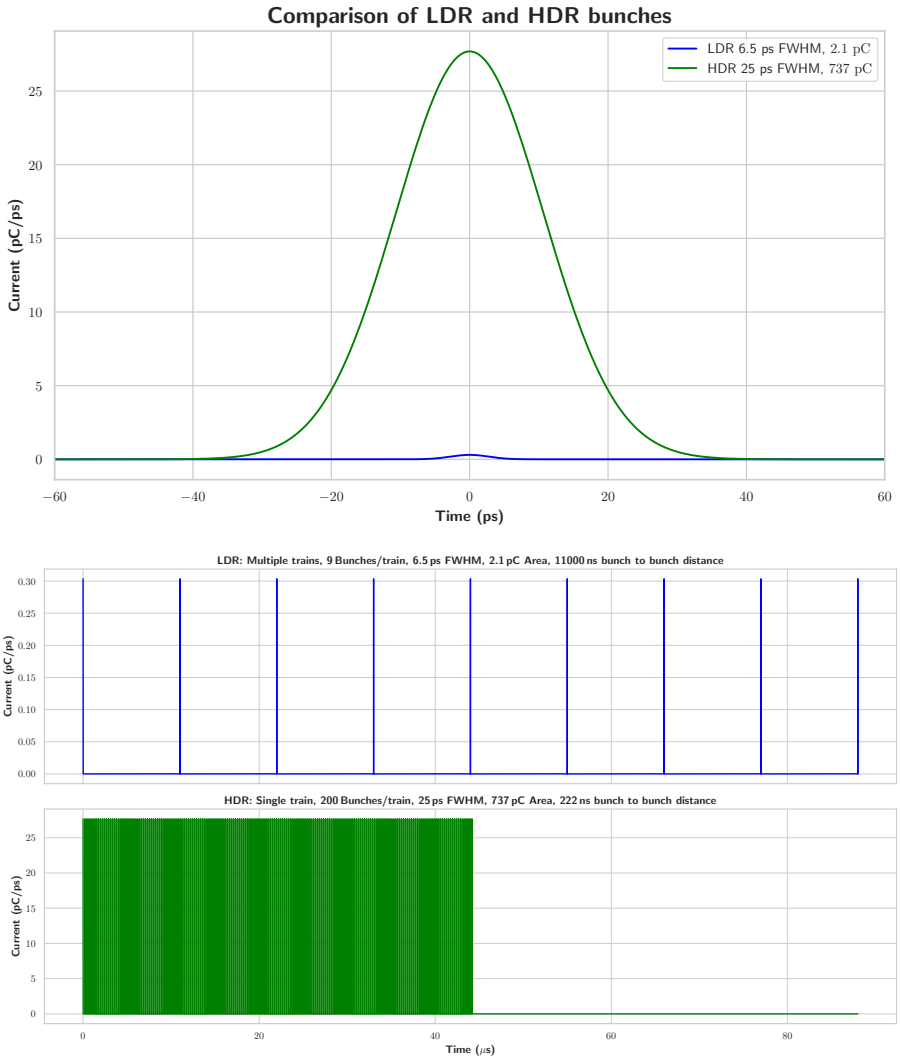

Figure S4: **Electron bunches and trains:** Comparison of LDR (blue) and UHDR (green) bunch (top) and bunch-train (bottom) structure in time. Note the differences in y axis scale.

The differences between simulated and measured doses (Fig. 5) are caused to a great degree from the deviation between the perfect ideal Gaussian form of the beam profile included in the simulation and the non-ideally and non-perfectly symmetrical distributed beam profiles throughout the experiments.

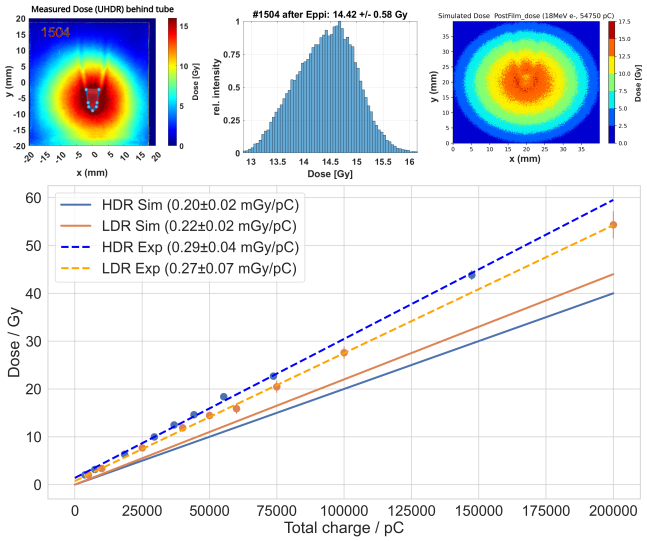

Figure S5: **Experimental and simulated doses:** Comparison of measured and simulated dose: Top left: Exemplary spatial dose distribution measured on a Gafchromic film behind the sample tube with 0.5 ml volume filled with 50 μL sample (left). The region of interest for sample dose determination is marked by light blue dots and lines. Top Center: Histogram of the dose distribution within the measured target volume in the sample tube as indicated by the blue lines in the image on the left. Top right: Simulated dose distribution within the same Gafchromic film as obtained by Geant4/Topas particle scattering simulations for the same conditions as in the experiment. Bottom: Shown is the dose deposit within the water volume for LDR (orange) and UHDR (blue) conditions in experiment (circles and a linear regression as broken lines) and simulation (solid lines) in dependence of the total charge.

These poseitions were monitored during the measurements by the Gafchromic films positioned before and after the sample and accounted for during the dose calculation per sample. The inverse difference per pC during the simulations is a result of the spatially broader beam for UHDR compared to LDR, and therefore a lower number of hits within the “target volume” represented by the water in the tubes.

5 Damage analysis of plasmid DNA by caplillary gel electrophoresis

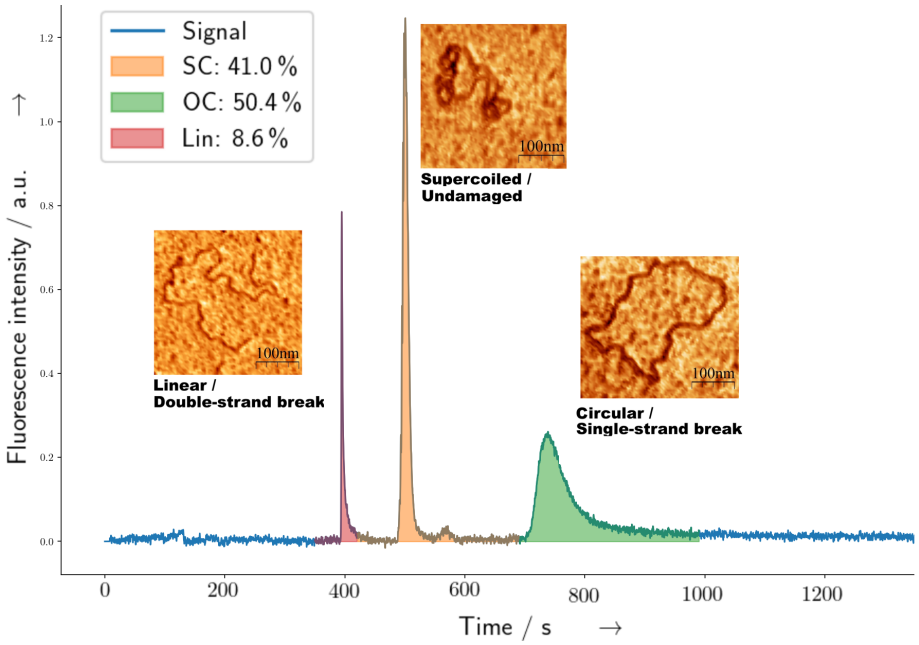

Figure S6: **Plasmid conformations, damage and their position in an exemplary CGE measurement.** Shown is a CGE densiogram of plasmid pUC19 with 2686 bp and three clearly visible isoforms. From left to right as linear (Lin: red, around 400 s), supercoiled/covalently-closed circular (SC: yellow, around 500 s) and open-circular (OC: green, around 750 s) conformation. To visualize the microscopic structure of the different plasmid DNA isoforms, atomic-force microscopy (AFM) images are shown as insets next to the respective band in the densiogram. The images were taken and combined with permission from previous works.[2, 3]

6 LET and energy spectra of the electron beam

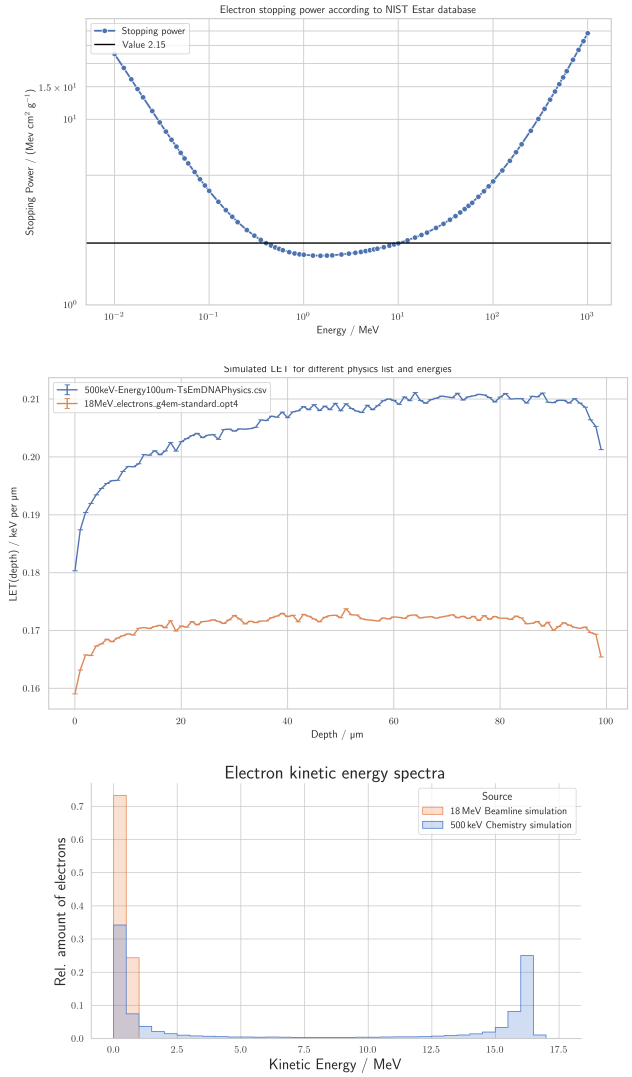

Figure S7: **Properties of the electron beam:** Energy dependent stopping power of electrons from the *NIST Elstar* database (top) and the related LET values (center) for different electron energies and simulation settings, and the respective kinetic energy spectra originating from particle scattering simulations (bottom).

7 Dosimetry and calibration procedure

Dosimetry during all irradiation experiments was performed using radiochromic films (Gafchromic EBT-XD, Ashland Inc., USA)[4], which provide high spatial resolution and are suitable for high-dose and ultra-high dose-rate (UHDR) applications. For each irradiation, one film was placed upstream and one downstream of the sample, enabling determination of the entrance and exit dose distributions and assessment of beam homogeneity across the irradiated volume. Films were scanned 24 hours post-irradiation using a calibrated flatbed scanner (Epson Expression 12000XL) under controlled and reproducible conditions. The pixel values from all three color channels were averaged to reduce channel-specific noise and improve signal stability. Regions of interest (ROIs) corresponding to the sample volume were defined based on the spatial beam profile, and the mean pixel value within each ROI was used for dose evaluation.

Initial calibration of the film response was performed under reference conditions using a clinical 6 MV photon beam, traceable to an ionization chamber standard and subsequently adapted to ultra-high dose-per-pulse (UHDR) beam delivery at the FLASHlab@PITZ beamline. The delivered dose per bunch (≈0.17–0.25 Gy/bunch) under UHDR conditions was independently estimated from beam parameters (charge range ≈550–820 pC, repetition rate 4.5 MHz, single-train operation), with transverse beam sizes of ≈2.8-3.9 mm and ≈3.1-3.6 mm. However, it is well established that radiochromic films may exhibit deviations from linearity, particularly at high doses and under UHDR conditions. Therefore, an empirical non-linear calibration was established using independent dose measurements obtained with a flashDiamond detector under comparable beam conditions to correct for dose-dependent response deviations of the radiochromic films in the investigated dose range (Fig. 8). The relationship between the flashDiamond dose and the corresponding Gafchromic film dose was described by a third-order polynomial shown in Eq. S.1:

$$D_{film} = A + B \cdot D_{fD} + C \cdot D_{fD}^2 + E \cdot D_{fD}^3 \tag{S.1}$$

with

$$A = 0.08568 \pm 0.04757$$

$$B = 0.91724 \pm 0.0314$$

$$C = 0.00401 \pm 0.00168$$

$$E = 2.88 \cdot 10^{-6} \pm 1.49 \cdot 10^{-5}$$

where A, B, C, and E are fit parameters obtained from least-squares regression. The cubic model was chosen as the lowest-order polynomial providing an adequate description of the observed non-linear behavior across the full dose range. This calibration describes the measured film response as a function of the independently measured flashDiamond dose. For subsequent dose correction, the polynomial relation was numerically inverted to obtain the corresponding physical dose from each measured film dose. The resulting fit showed

excellent agreement with the experimental data (coefficient of determination $R^2 = 0.99913$, adjusted $R^2 = 0.99884$), indicating that the model captures the dominant features of the film response. The deviation from linearity becomes increasingly pronounced at higher doses, consistent with previously reported behavior of radiochromic films in high-dose and UHDR regimes.[5] The calibration function was inverted and applied consistently to all film measurements to obtain corrected dose values used in the subsequent analysis. It should be noted that the calibration model is empirical and valid within the investigated dose range. Extrapolation beyond this range is not justified. The uncertainty of the corrected dose D_{real} was determined by propagating the uncertainties of both the calibration parameters and the measured film dose using standard Gaussian error propagation. For the calibration model given above, the total uncertainty is expressed as in Eq.S.2:

$$\sigma^2_{D_{film}} = \sigma^2_A + (D_{fD}\sigma_B)^2 + (D^2_{fD}\sigma_C)^2 + (D^3_{fD}\sigma_E)^2 + [(B + 2CD_{fD} + 3ED^2_{fD})\sigma_{D_{fD}}] \tag{S.2}$$

Where σ_A, σ_B, σ_C, and σ_E are the standard uncertainties of the fit parameters, and is the standard uncertainty of the flashDiamond dose measurement. The propagated uncertainties are reflected in the calibration uncertainty band shown in Fig. 8. For correction of experimental film measurements, the calibration relation was numerically inverted to obtain the corresponding corrected physical dose D_{real} from each measured film dose D_{film}. The uncertainty of D_{real} was then obtained by propagating the measured film-dose uncertainty through this inverse relation. Therefore, the uncertainty in the corrected dose includes contributions from the film measurement uncertainty and from the empirical calibration model. This formulation accounts for the dominant dependence of the corrected dose on both the polynomial coefficients and the measured signal. As a consequence, the resulting uncertainty is inherently dose-dependent. At low doses, the uncertainty is dominated by the constant and linear terms of the calibration function, whereas at higher doses, contributions from the quadratic and cubic terms become increasingly significant. In particular, at doses above approximately 40–50 Gy, the uncertainty is primarily driven by the higher-order terms, reflecting the increased sensitivity of the correction to the non-linear response of the film. The applied calibration procedure is based on an empirical model that captures the observed non-linear response of the Gafchromic films under the specific experimental conditions used in this study. While the agreement with independent detector measurements supports the validity of this approach, several limitations should be noted. First, the calibration does not explicitly account for potential variations in film response due to differences in dose-per-pulse or instantaneous dose rate beyond those captured in the empirical fit. Second, correlations between fit parameters were not explicitly included in the analytical uncertainty propagation, which may lead to a conservative overestimation of the total uncertainty depending on their covariance. Third, the model does not incorporate potential systematic effects related to

environmental conditions, film batch variability, or long-term scanner stability. However, all films used in this study were obtained from the same production batch, and scanner performance was regularly verified under consistent operating conditions, thereby minimizing these sources of variability. Despite these limitations, the consistency of the corrected dose values with independent measurements and the systematic application of the same calibration procedure to all datasets ensure that relative comparisons between different irradiation conditions remain robust.

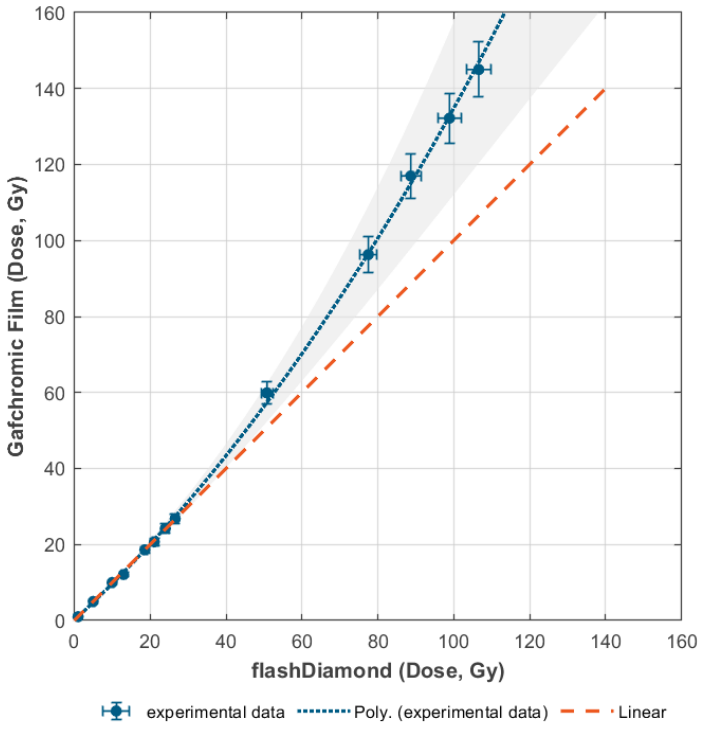

Figure S8: Calibration of Gafchromic EBT-XD film response against flashDiamond dose measurements. Blue markers represent the experimental calibration data, with horizontal and vertical error bars corresponding to the standard uncertainties of the flashDiamond and film dose measurements, respectively. The blue dotted curve shows the cubic polynomial fit used to describe the nonlinear film response, while the orange dashed line represents the hypothetical linear response. The grey shaded region indicates the propagated standard uncertainty of the cubic fit for a coverage factor. The widening of the uncertainty band at higher doses reflects the increasing contribution of the higher-order terms in the empirical calibration model.

8 Correction of the measured doses during the irradiation experiments

Following from the procedure outlined in the previous chapter, the nonlinear response of the Gafchromic films in the present high-dose rate regime can be corrected by the following function:S.3

$$D_{real} = 0.0000118 \cdot D_{film}^3 - 0.00406 \cdot D_{film}^2 + 1.07732 \cdot D_{film} - 0.07943 \quad \text{(S.3)}$$

Hereby the D_{film} is the measured dose from the Gafchromic films, while D_{real} represents the physical dose as used in the analysis of the data in the main manuscript. A representative image of the Gafchromic films and the homogenious exposure can be found in Fig. 5.

9 Visualization of the simulated geometry

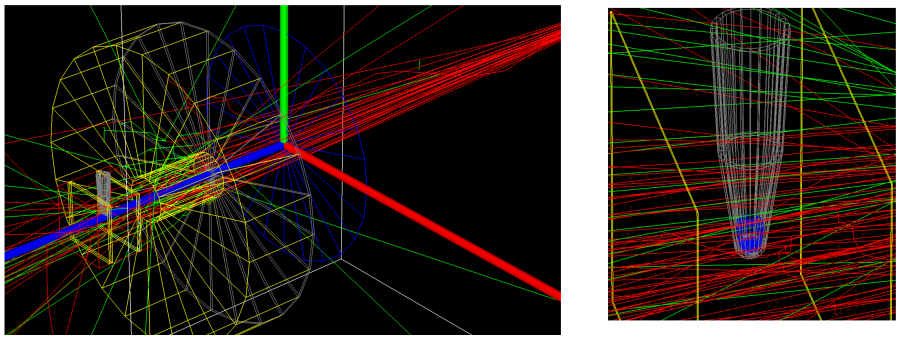

Figure S9: Left: Particle scattering simulations showing the simulated setup. Hereby electrons are shown in red, photons in light green. Sample tubes are grey, water blue, Gafchromic films before and behind the samples are shown in yellow. Before them, the scattering plate in blue and the lead shielding with a hole are shown in yellow. The image in the center right, shows a zoom to the sample tube and Gafchromic films. The electron beam propagated from right to left and for illustration purposes the number of electron simulated is strongly reduced with respect to the real case. Bottom: Shown is the dose deposit within the water volume for LDR (orange) and UHDR (blue) conditions in experiment (circles and a linear regression as broken lines) and simulation (solid lines) in dependence of the total charge.

Supplementary References

[1] S. R. McKeown, *British Journal of Radiology* **2014**, *87*, 20130676.

[2] L. Cordsmeier, M. B. Hahn, *ChemBioChem* **2022**, *23*, e202200391.

[3] M. B. Hahn, *Sci Rep* **2025**, *15*, 1068.

[4] A. L. Palmer, A. Dimitriadis, A. Nisbet, C. H. Clark, *Phys. Med. Biol.* **2015**, *60*, 8741.

[5] F. Horst, A. Schüller, R.-P. Kapsch, T. Hackel, J. Pehlivan, C. Schott, E. Beyreuther, J. Pawelke, *Phys. Med. Biol.* **2026**, *71*, 045020.